A DUAL-POLARIZATION INVESTIGATION OF TORNADO WARNED CELLS ASSOCIATED WITH HURRICANE RITA (2005)

Christina C. Crowe* +, Walter A. Petersen^, Lawrence D. Carey+
+University of Alabama, Huntsville, Alabama
^NASA Marshall Spaceflight Center, Huntsville, Alabama

1. INTRODUCTION

The 2005 Hurricane season was the most active Atlantic hurricane season on record and boasted four category 5 strength hurricanes (Emily, Katrina, Rita and Wilma). Of those storms, Hurricane Katrina garnered most of the attention during the 2005 season. But less than a month after Katrina made landfall on the Gulf Coast, Rita caused additional devastation over much of the same region. Hurricane Rita spurred one of the largest evacuations in US history, with possibly over two million evacuees from Texas alone (Beven et al. 2008). A significant tornado outbreak, which was also associated with Rita and contributed to an increased danger further inland, is the focus of this study.

Overall, Hurricane Rita directly caused seven fatalities and indirectly led to another 55 casualties. In addition, $11.4 billion in damage was caused by the storm as a whole (Beven et al. 2008). Specifically, the damage associated solely with the Hurricane Rita tornadoes (Table 1) totals $18.4 million. When looking at these statistics, one can pose a question about the relevance of a study on hurricane tornadoes when they are only responsible for less than 1% of the total damage caused by a hurricane. When the total amount of damages by state is considered, the relevance is made abundantly clear. While the coastal regions, in this case, incur damage almost solely due to the storm surge and high winds, locations further inland have a much higher risk of damage due to the tornadoes spawned by the storm. In the case of Hurricane Rita, one-third of the damage in Arkansas, one-half of the damage in Mississippi, and almost all (99%) of the damage in Alabama was caused by tornadoes. The tornadoes were also responsible for one of the seven deaths attributed to the storm.

**Corresponding author address:* Christina C. Crowe, NSSTC, 320 Sparkman Dr., Huntsville, AL 35758; e-mail: Christina.Crowe@noaa.gov

One hundred and three tornadoes associated with Rita were reported across the Southeast between her landfall and transition to extra-tropical cyclone. Throughout this time, the National Weather Service offices across the Southeast issued a total of 533 warnings with a Probability of Detection (POD) of 0.87 and False Alarm Rate (FAR) of 0.84. This study is part of a larger project that intends to examine the forecast process from event preparation through warning operations to identify tools or storm characteristics forecasters will be able to use in warning operations. This will aid in cutting down on tornadic FAR in hurricane landfalling systems.

This paper will examine only the dual-polarimetric radar analysis portion of the larger, multi-faceted study on Hurricane Rita. The following section will discuss previous dual-polarimetric radar studies of severe and tornadic storms. Section 3 includes information on data sources and analysis methods used in this study. The analysis and results found during this research are presented in Section 4. Finally, Section 5 summarizes the results of this study and presents conclusions drawn from this research.

2. BACKGROUND

A handful of studies have investigated the evolution of dual-polarimetric characteristics in tornadic and non-tornadic storms. Dual-polarimetric variables provide unique and valuable insights into the microphysical processes occurring during the development of storms (Kumjian and Ryzhkov 2007 and Romine et al. 2008). The three main variables discussed in the literature and in this paper include standard radar reflectivity or horizontal reflectivity (Z_H), and the dual-polarimetric variables differential reflectivity (Z_{DR}) and specific differential phase (K_{DP}). Z_H is the standard horizontal polarization reflectivity from basic radars and higher values are an indicator of stronger rainfall or hail, but alone

State	Torn.	Fatal.	Injur.	Tornado Dmg	Tot. Rita Dmg	%
Alabama	23	0	2	$1,362,000	$1,371,000	99.34
Mississippi	54	1	13	$14,578,000	$30,845,000	47.26
Arkansas	18	0	5	$685,000	$2,075,000	33.01
Louisiana	8	0	3	$1,748,000	$4,490,000,000	0.04

Table 1. *Breakdown by state of number of tornadoes, and fatalities and injuries directly associated with the tornadoes. Damage due solely to tornadoes and overall damage sustained from Hurricane Rita are broken down by state and the percentage of total damage caused by tornadoes is given. (NCDC 2009)*

cannot be used to differentiate the two. Z_{DR} is a ratio of reflectivity returned in the horizontal (Z_H) and vertical (Z_V) polarizations and gives reflectivity-weighted information about drop size. It is computed using

$$Z_{DR} = 10\log\left(\frac{Z_H}{Z_V}\right) \quad (2.4.)$$

Typical values of differential reflectivity are from -2 dB to 6 dB for a C-band radar and will vary depending on the frequency of the radar used.

K_{DP} can be estimated by taking the range derivative ($r_1<r_2$) of differential phase (Φ_{DP}), which is defined as the difference between the phase of a horizontally-polarized return and the phase of a vertically-polarized return signal. It can be calculated using

$$K_{DP} = \frac{\phi_{DP}(r_2) - \phi_{DP}(r_1)}{2(r_2 - r_1)} \quad (2.5.)$$

A benefit of using this term is system noise and backscatter phase are removed. Typical values of specific differential phase are -1 $°\,km^{-1}$ to 6 $°\,km^{-1}$, but this parameter is also frequency-dependent.

Because larger rain drops are more oblate and have an increased horizontal axis, increasing values of Z_{DR} indicate larger drop sizes whereas values near zero indicate spherical hydrometeors such as small raindrops (when co-located with small Z_H) or large hail (when co-located with large Z_H). K_{DP} is related to axis ratio of hydrometeors, and therefore to drop sizes as is Z_{DR}. But K_{DP} is also related in a more formal definition to concentration of droplets and therefore to liquid water content (W). Essentially, K_{DP} is proportional to W times the mass-weighted mean diameter of the hydrometeors in the volume (D_m). When K_{DP} fields are used in concert with Z_{DR} fields, rainfall rates can be better estimated. For example, regions with smaller raindrops and larger liquid water content can be identified by increasing values of K_{DP} and decreasing values of Z_{DR} (e.g., Petersen et al. 1999).

A number of recent studies (Romine et al. 2008 and Kumjian and Ryzhkov 2008, 2009) have identified a Z_{DR} arc signature, in the lowest 1 km, associated with both tornadic and non-tornadic storms. This signature occurs on the right side of cells along the Z_H gradient and often has values greater than 5 dB, with values greater than 6 dB in tornadic cases (Kumjian and Ryzhkov 2008). This enhanced Z_{DR} is a sign of locations of weaker vertical velocities outside of the main core updraft of the cell. Size sorting of hydrometeors occurs because a strong updraft is needed to support large raindrops or hail; with a weaker updraft these drops can more easily make it to the surface. The arc shape to this enhanced Z_{DR} has only been noted in severe storms and may be evidence of a veering in the winds with height. Therefore, this Z_{DR} arc may also be an indicator of storm relative helicity (SREH) strength (Kumjian and Ryzhkov 2007, 2009).

From these differences in updraft strength and vertical shear, size sorting of raindrops occurs. Smaller raindrops, which take longer to fall, are advected further downwind in the cell and larger drops are able to fall out just outside of the updraft core (Kumjian and Ryzhkov 2007, 2008). The resultant fields in dual-polarimetric variables from this size sorting process include enhanced Z_{DR} along the right flank of the cell during its mature phase, while increased K_{DP} values appear in the forward flank of the cell and further to the left from the Z_{DR} arc (Fig. 1).

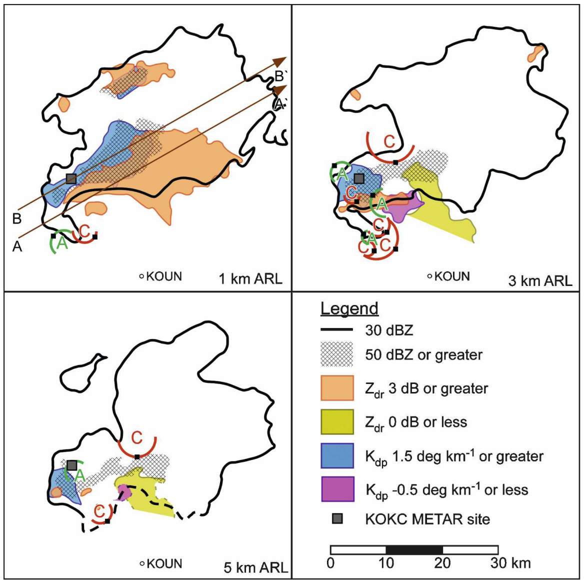

***Fig 1.** CAPPI plot at 1 km (top left), 3 km (top right) and 5 km (bottom left) ARL (above radar level) at 2204 UTC on 8 May 2003, near Oklahoma City, OK. Contours and shading done according to the inset legend. Half circles with the letter A indicate a region of anticyclonic rotation while half circles with the letter C indicate regions of cyclonic rotation. Small black boxes indicate couplet alignment relative to the radar. A tornado was reported at 2206 UTC (Figure 12 from Romine et al. 2008).*

Kumjian and Ryzhkov (2009) performed a modeling study to test the resulting dual-polarimetric fields associated with variations in wind shear. It was found that increased size sorting occurs as storm-relative wind speeds and directional shear increase. But unidirectional shear in the environment of their modeled cells only led to Z_{DR} enhancements and not the arc shape, which should be located along the front right edge of the cell along the reflectivity gradient associated with the forward flank downdraft and parallel to storm motion. When directional shear was added to the environmental profile, a Z_{DR} arc appeared in the modeled cell, with a positive correlation between increased directional shear and more substantial Z_{DR} signatures. Therefore it has been suggested localized enhancements of SRH can be identified by increased Z_{DR} values in the arc.

Only a few clear differences between tornadic and non-tornadic storms from a dual-polarimetric perspective have been determined thus far. Kumjian and Ryzhkov (2008) discuss that tornadic storms tend to pull the Z_{DR} arc into the hook echo whereas non-tornadic cells do not. In addition, Kumjian and Ryzhkov (2009) noted that the Z_{DR} arc signature was more often interrupted after mesocyclone occlusion by hail signatures in non-tornadic cells. Kumjian and Ryzhkov (2008b) compare inferred drop size distributions (DSDs) in tornadic versus non-tornadic storms and conjecture from radar that non-tornadic hooks (i.e., near the core of the storm) have larger drop sizes than tornadic hook echoes. They identify this as important for thermodynamic attributes of the storm flow, as larger drops indicate greater evaporation of smaller drops in the volume. Increased evaporation provides more cooling in the downdraft, resulting in a greater difference between rear-flank downdraft (RFD) temperatures and that of the surrounding environment. While some cold pool from the downdraft is needed, Markowski et al. (2003) also note that RFDs with too large of a temperature deficit do not allow for significant recycling of parcels. Slightly warmer parcels can be recycled into the updraft and retain or increase low-level vertical velocities. This evidence indicates that there may be an ideal range of temperature differences between the RFD and environment and therefore an associated ideal range for Z_{DR} values in the arc.

One indicator that Kumjian and Ryzhkov (2008) present that has a zero FAR for tornadic storms is the Tornadic Debris Signature (TDS). But they discuss no POD for this type of indicator. The TDS is a region with high Z_H, low Z_{DR}, and very low ρ_{HV}, but it cannot identify weaker tornadoes or those that go over open fields and do not pick up debris. The occurrence of a TDS requires less than common circumstances and a low POD is expected, for this reason the TDS was not investigated for this study. Many researchers agree that a larger dataset of storms, both tornadic and not, is needed to determine any more concrete differences between these types of storms from a dual-polarimetric standpoint.

One concern about comparing hurricane tornadoes to Midwest polarimetric studies is due to the fact that landfalling hurricane environments are characterized by high shear and low to moderate CAPE, which differs from classic Midwest tornadic outbreak environments that tend to benefit more from high CAPE values. But the high shear and low CAPE environment does define cold season tornado outbreaks (Kumjian and Ryzhkov 2008) and a number of dual-polarimetric studies have looked at these types of tornadoes. Kumjian and Ryzhkov (2008) looked at the persistence of the hail signature in tornadic versus non-tornadic storms in the cold season. They noted that Z_{DR} values near zero associated with high Z_H (hail signature) were fairly consistent in non-tornadic storms. Since updraft weakening has been considered a precursor of tornado production and weaker updrafts cannot support continued hail production, this lack of a consistent hail signature in a tornadic cell correlates well with this understanding.

3. DATA AND METHODOLOGY

ARMOR is located at the Huntsville International Airport 34.649° latitude and -86.771° longitude (Fig. 2). Specifications for this C-band radar were discussed by Petersen et al. (2005). During the period of the study, ARMOR's scan strategy was set at RAIN1 which performs scans at three elevation angles: 0.7°, 1.3° and 2°. This scan is set to be executed at an interval of 5 minutes, but at times during the event they were run back-to-back, providing new volume scans up to every 2 minutes. ARMOR provides information on numerous single- and dual-polarization variables, but those discussed in this study include Z_H, v_r, Z_{DR}, and K_{DP}.

While one would prefer to have had full volume ARMOR scans for this study, these lower levels still provide valuable data in tropical settings due to the more shallow characteristics of tropical supercells (McCaul and Weisman 1996). In addition, this research focused on the operational uses of the information in the study. In rapidly evolving situations, forecasters generally utilize the lowest level scans to make initial warning decisions; therefore any keys found in these levels may provide the timeliest indicators of tornadogenesis for forecasters. Also, Kumjian and Ryzhkov (2008) used these lowest elevation angles in order to determine near surface conditions in the tornadic environment.

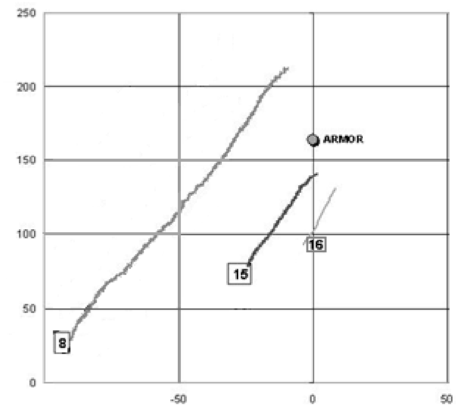

Figure 2. Track of three storms used for dual-polarimetric study and the location of ARMOR. Grid units are in km.

The data were edited with the NCAR SOLOII software. Editing primarily focused on the unfolding of v_r data. After this was performed, REORDER, another NCAR program, was used to grid the data with a Cressman weighting function. The data was gridded to a three-dimensional Cartesian grid, centered on the ARMOR radar location, with 1 km horizontal resolution, from which constant-altitude plan position indicators (CAPPIs) were produced for 6 levels with a resolution of every 1 km in the vertical. These lower levels were used to focus on the lower levels of these storms.

Time-height plots were created for each cell lifetime to look at storm development. It should be noted that the plotting program, GRI, uses a Barnes analysis when plotting the columnar time-step data into a gridded image. Errors associated with this analysis were found to be less than ten percent on the edges of the grid. While an acceptable error, this was taken into consideration when analysis of these plots was performed.

4. ANALYSIS

Nineteen warnings were issued by WFO HUN during the course of the Hurricane Rita outbreak. In order to determine the cells that would be best for the dual-polarimetric study, the warnings were first filtered by their location relative to ARMOR. Information from warning text about the location of cells that prompted the warnings and their updates was compared to radar

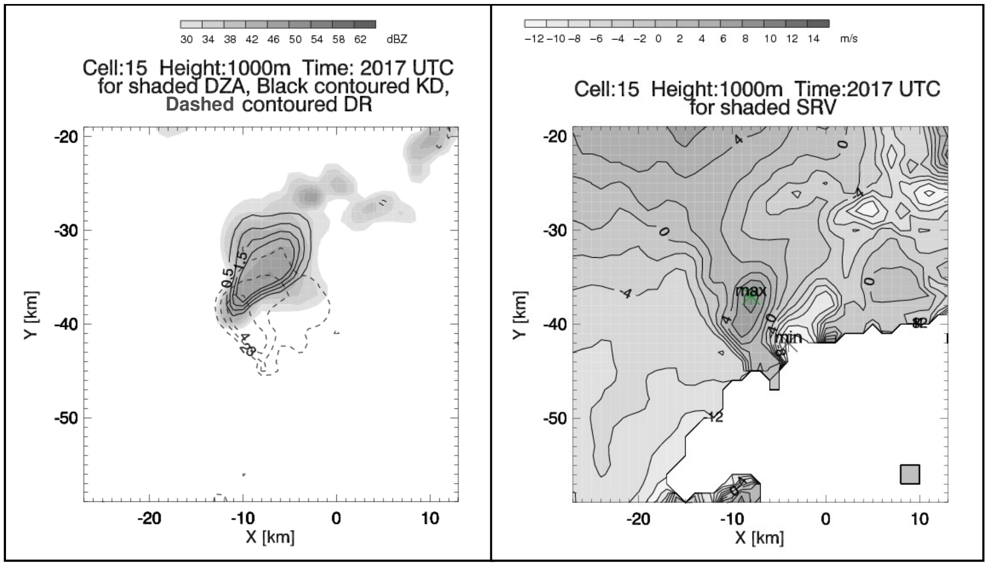

Figure 3. Radar polarimetric variables for Cell 15 at 2017 UTC 25 Sept., shown on a 1-km CAPPI: (a) reflectivity factor (Z_H; listed as DZA in image; dBZ) is shaded every 4 dBZ beginning at 30 dBZ, differential reflectivity (Z_{DR}; listed as DR in image, dB) is dashed contoured every 1 dB from 2 – 5 dB, specific differential phase (K_{DP}; listed as KD in image, °km^{-1}) is solid contoured every 0.5 °km^{-1} from 0.5 to 2.0 °km^{-1}, and (b) storm relative Doppler velocity (SRV; m s^{-1}) is contoured and shaded every 2 m s^{-1}.

reflectivity around the warning periods. This was done to identify warnings associated with particular cells and then manually track those cells through their lifetime. Tornado reports from NCDC were dealt with similarly to give a full picture of the threat associated with each cell. From this analysis, it was determined that three particular cells traversed close enough to ARMOR to provide detailed analysis of the lower levels. Details on each cell follow.

The initial cell of interest warned on (Cell 15) prompted the first warning by WFO HUN at 2012 UTC 25 Sept. for Cullman County, AL. Two additional warnings were issued for Morgan County (2019 UTC) and Madison County (2041 UTC) as it moved northeastward. Two separate reports were received, one was a tornado report north of Cullman, AL, in Cullman County at 2018 UTC, and another was for a funnel cloud east of Falkville, AL, in Morgan County at 2030 UTC.

The first warning issued for the second cell of interest (Cell 8) was for Limestone County at 2100 UTC. Two additional warnings were issued for Limestone County at 2127 UTC. It should be noted that the second of these two additional warnings was intended as a correction to the first additional warning, but an error led to the correction being categorized as a new warning. This second warning is not included in official statistics. The forecaster was attempting to fix an incorrect location in the text of the first warning issued 2127 UTC. This storm traversed northeastward across the county and had a funnel cloud report north of Tanner, AL, in Limestone County at 2115 UTC. No tornado was reported with this storm within range of the ARMOR radar.

The last cell of interest (Cell 16) approached Cullman County and at 2117 UTC the first warning was issued for the storm. This storm also progressed northeastward and into Morgan County before weakening. There were two additional warnings for the storm in Morgan County at 2139 UTC and 2216 UTC. No funnel or tornado reports were associated with this cell.

Cell 15 showed an organized structure as it developed into a mature supercell. Through the development into the mature phase of the storm, a distinct separation of Z_{DR} and K_{DP} maxima could be observed (Fig. 3). The K_{DP} maximized in the forward flank of the storm, downshear of the main updraft of the storm. Meanwhile, the Z_{DR} maximized on the right and rear of the cell and is wrapped around the back side of the updraft with values up to 8 dB and around 6 dB at the time of the tornado. These two characteristics of the K_{DP} and Z_{DR} maxima reflect the size sorting associated with strong mesocyclone development discussed above. Just prior to the tornado report in Cullman County, the Z_H became pinched and the v-notch shape of the forward flank began to erode indicating the occlusion of the mesocyclone associated with the cell.

After the time of the tornado, there was an increase in Z_H in the storm at lower levels (1km) and that maximum began to become collocated with the relative maxima in K_{DP} and Z_{DR} (Fig. 4). The increase in Z_H began at 2014 UTC, just prior to the tornado report, and lasted through 2024 UTC, with an increase of 6 dB. While this is not a large difference in reflectivity, for the 30 minutes prior to this period, the maximum reflectivity had been fairly steady state (Fig. 5 and 6). This sudden increase in low-level reflectivity suggests that updraft in the storm was beginning to collapse.

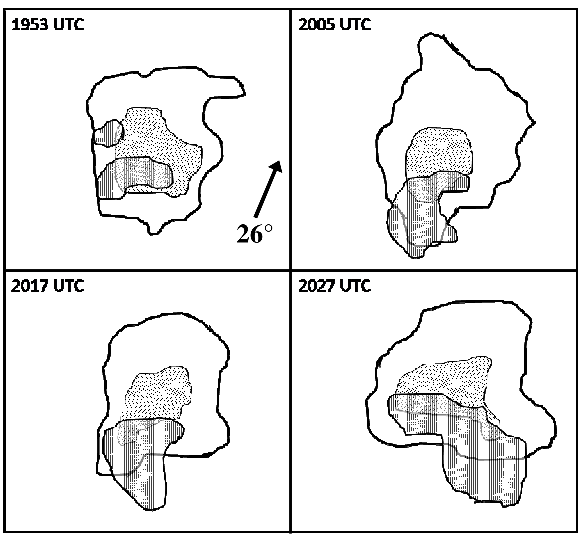

Fig. 4. *Time series for Cell 15 at 1953 UTC (top left), 2005 UTC (top right), 2017 UTC (bottom left), and 2027 UTC (bottom right). The thick black line indicates the 30 dBZ reflectivity contour, the region filled with vertical stripes indicates differential reflectivity values greater than 3 dB, and speckled region indicates specific differential phase values greater than 1.5 °km^{-1}. Direction of storm motion indicated by arrow in first panel.*

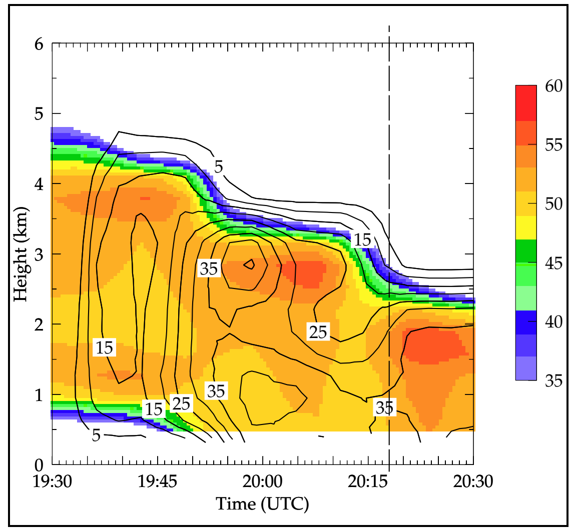

Fig 5. *Time-height analysis for Cell 15 from 0.5 to 6 km of maximum reflectivity (dBZ – shaded from 35 – 60 dBZ according to color bar on right) and angular momentum (m s^{-1} km – contoured in black). Tornado time is indicated by the vertical dashed line. Missing data is left shaded white. Data from ARMOR radar was limited only to the lower levels and no data from other radars was available to supplement the upper level data. The gradient on the upper edge of the shading, therefore, is likely an artifact of missing data. Cell 15 is 89 km from ARMOR at the beginning of the period, is 60 km away at 2000 UTC, and is 23 km away at the end of the period.*

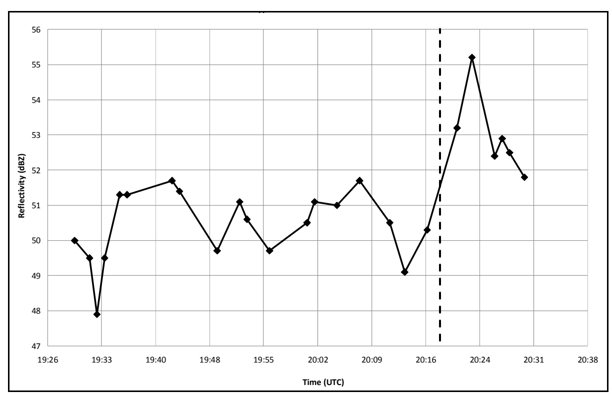

Fig. 6. *Trend of maximum reflectivity value in Cell 15 over time (in black) at 1km altitude. The dashed line indicates the time of the tornado report in Cullman County.*

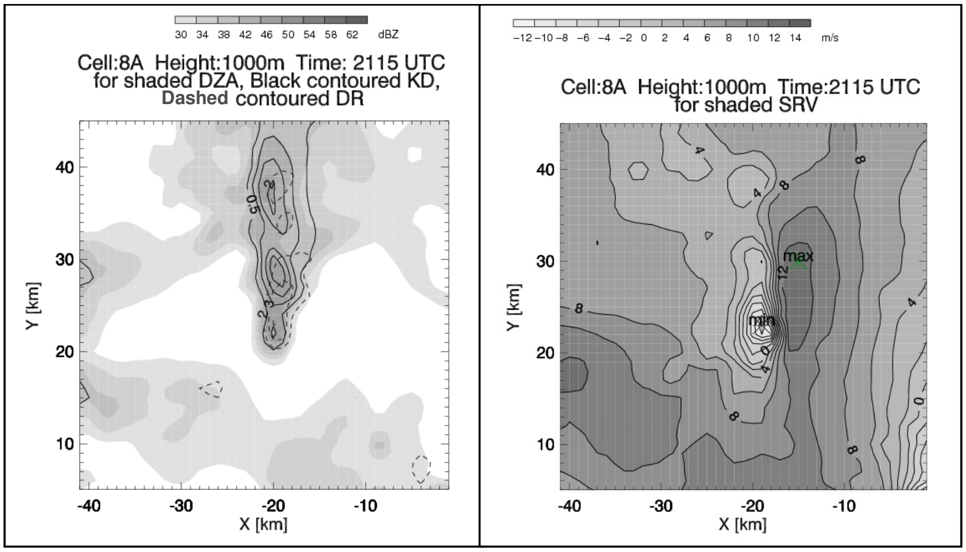

Figure 7. Same as Figure 3 except for Cell 8 at 2115 UTC 25 Sept.

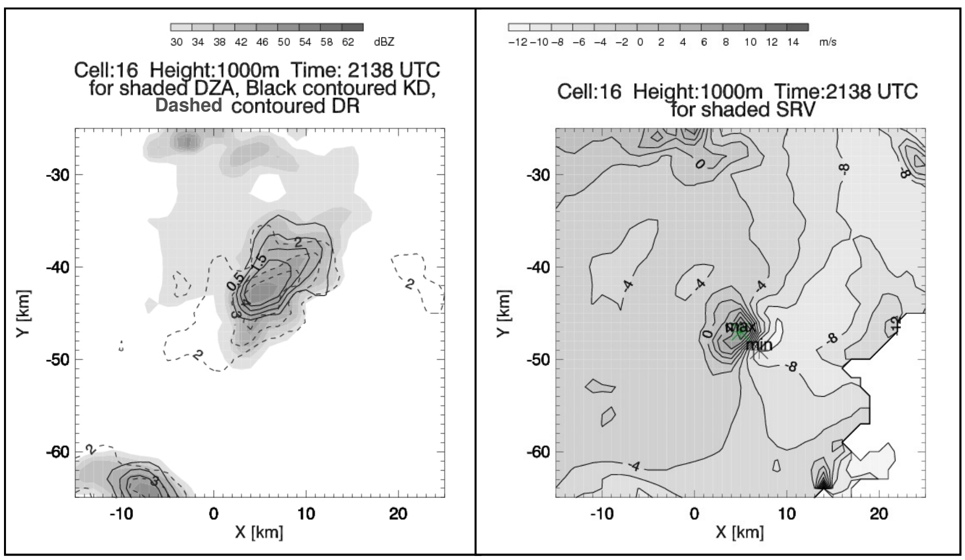

Figure 8. Same as Figure 3 except for Cell 16 at 2138 UTC 25 Sept.

With a collapse in the updraft, larger raindrops would be able to fall to the surface, increasing the Z_H, and the size-sorting previously provided by the rotating updraft would desist, as evidenced by the lack of separation between K_{DP} and Z_{DR}. This increase in Z_H associated with the collapsing updraft and resultant tornadogenesis has also been noted by Romine et al. (2008) and Kumjian and Ryzhkov (2008).

Cell 8 exhibited a more linear structure than Cell 15. The polarimetric variables and radial velocity at the time of the funnel report in Limestone County (Fig. 7) showed only a slight Z_{DR} preference to the right rear of the storm. Additionally, there was slightly more overlap between K_{DP} and Z_{DR} maxima both at this time and over the lifetime of the storm in general. Weaker vertical shear than in the Cell 15 may be occurring at that time since there is less separation between these maxima. In addition, Z_{DR} values for the Limestone cell remain below 5 dB with only a slight increase around the time of the funnel cloud.

This indicates a weaker updraft that was unable to generate larger raindrops. Strengthening or weakening of the updraft cannot be inferred around the time of the funnel report, as maximum Z_H values remained fairly consistent over a thirty minute period surrounding the funnel report.

Cell 16 had a structure similar to Cell 15 in that it had a more discrete supercellular type structure in Z_H, but the polarimetric structure was vastly different. This cell had even less sorting of drop size distribution, as can be seen from the co-location of the K_{DP}, Z_{DR}, and Z_H maxima. At the time of the second warning issued for the storm (Fig. 8), a slight v-notch was evident in the reflectivity. Velocity values indicated a strong mesocyclone, which likely prompted the warning. But while a marginal preference for larger drops and water-coated hail (greater K_{DP}, Z_{DR}, and Z_H) towards the right flank of the storm could be seen, there were overlapping bulls-eyes of all three values over the same region. Z_{DR} values around this time were not as high as near the Cell 15 tornado report, but still hovered around 5 dB.

Significant differences in size sorting can be seen among these cells. As evidenced by more overlap of K_{DP}, Z_{DR}, and Z_H for Cells 8 and 16 compared to Cell 15, size sorting through lofting smaller drops further downwind was not able to occur. Additionally, the Z_{DR} maximum was pushed further downwind of the core as compared to Cell 15, which suggests that large and small drops alike are being pushed equally far from the core. One explanation for this difference in size sorting could be that vertical shear was not as strong as in Cell 15 (Kumjian and Ryzhkov 2008). While other size sorting processes could be the culprit, these indicators could suggest that a difference in vertical structure of tornadic storms could be the key to detection.

To summarize these dual-polarimetric findings, each of these cells were compared and contrasted to the fields observed by Romine et al. from near a tornadic period (Fig. 1). Each of the cells were analyzed around warning and tornado report times and simplified images comparable to the Romine figure were created (Fig. 4, 9-10). It can be seen in the case of a tornadic cell, Cell 15 showed a separation of Z_{DR} and K_{DP} values, with high Z_{DR} preferred towards the right rear of the storm (Fig. 3). The Z_{DR} arc became more separated from the K_{DP} maximum and shifted further to the right rear along the Z_H gradient approaching and at the time of the tornado (2005 and 2017 UTC respectively).

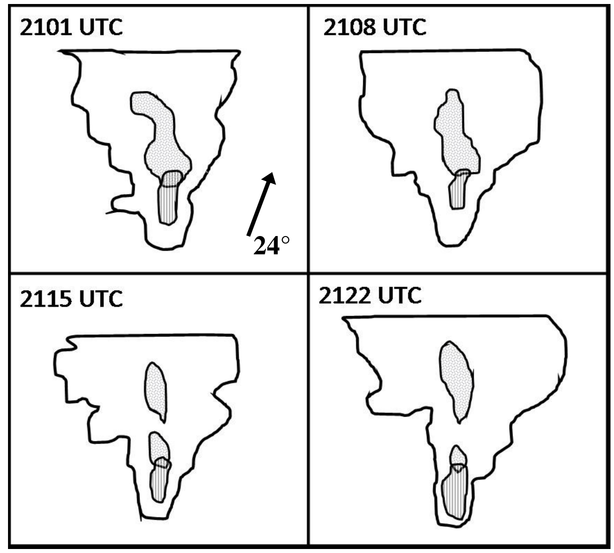

***Fig. 9**. Time series for Cell 8 at 2101 UTC (top left), 2108 UTC (top right), 2115 UTC (bottom left), and 2122 UTC (bottom right). Same shading as Figure 4.*

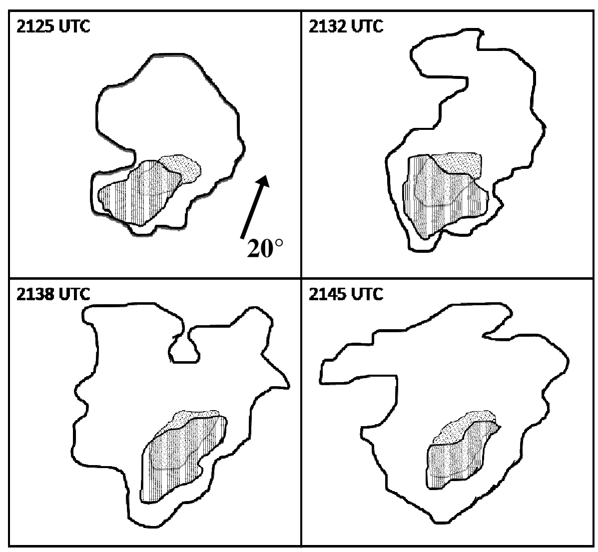

***Fig. 10**. Time series for Cell 16 at 2125 UTC (top left), 2132 UTC (top right), 2138 UTC (bottom left), and 2145 UTC (bottom right). Same shading as Figure 4.*

In addition, the arcing shape, as opposed to a more linear structure, to the enhanced region of Z_{DR} in Cell 8 (Fig. 9) suggests that greater SRH (Kumjian and Ryzhkov 2009) occurred in the near-storm environment of Cell 15 whereas Cell 8 was moving into a more unidirectional speed shear region identified in the BNA sounding. Cell 15 also shows greater horizontal separation between the enhanced Z_{DR} and K_{DP} regions than Cell 16 (Fig. 10) did over the period studied.

When analyzing these general figures, it should be noted that comparing Z_H contour shape to that of the Romine image will likely hinder an understanding of this dual-polarimetric analysis. The reader should keep in mind that cases studied in the referenced papers are associated with more classic Great Plains style structure that often displayed an obvious hook or appendage signature. Because supercells associated with tropical cyclones are smaller (mini-supercells), these signatures are less often sampled by radars. This leads to some of the difficulty in making warning decisions with these cases. Since the dual-polarimetric fields are similar to those seen in the more classic set-ups even while their basic reflectivity patterns are not, this may further enforce the utility of dual-polarimetric analysis in TC tornado cases. It should also be noted that even the modeling studies referenced in this paper have not fully taken into account a detailed understanding of microphysical processes occurring in these storms (Kumjian and Ryzhkov 2009). It would be beneficial in the future to perform a study that would analyze precipitation processes and drop trajectories using a Lagrangian framework.

5. SUMMARY AND CONCLUSIONS

Hurricane Rita's tornadoes provided a significant challenge to forecasters at the National Weather Service, including those in north central Alabama. While not unusual for landfalling hurricane cases, which are notoriously difficult warning situations, the verification statistics from this case lead to inquiries about what could be done with technologies that will be available in the near future to improve upon warning capabilities.

From the three cells investigated in northern Alabama, distinct differences in the microphysical processes occurring within each storm can be identified through dual-polarimetric analysis. In the storm that produced the tornado in Cullman County (Cell 15), a horizontal displacement of the maximum Z_{DR} and K_{DP} values suggests size sorting of hydrometeors due to a stronger updraft that begins to collapse in addition to increased directional shear within the storm. The other two non-tornadic storms display more co-located maxima of Z_{DR} and K_{DP} and smaller changes in Z_H over time which indicates a lack of significant updraft strengthening or collapse. These findings agree with previous dual-polarimetric studies on tornadic storms.

Of the few previous distinctions made between tornadic and non-tornadic cells, Kumjian and Ryzhkov's (2008) determination that Z_{DR} values of greater than 6 dB were associated with tornadic cells also holds in our Hurricane Rita cells studied, with the tornadic cell consistently at or above this value. The tornadic storm also exhibits Z_{DR} being wrapped around the back side of the updraft, which agrees with previous observations of Z_{DR} being pulled into the hook (Kumjian and Ryzhkov 2008) even though in this case no obvious hook is evident in the reflectivity field. Also, there was a noticeable lack of Z_{DR} holes in the lower level fields, agreeing with Kumjian and Ryzhkov (2008) and their finding that tornadic cells tend to lack a consistent hail signature of Z_{DR} values near zero.

The findings from this study suggest that warning operators can benefit dual-polarimetric technology that will be operational nationwide in the near future. The separation of dual-polarimetric values which suggest enhanced size sorting within tornadic supercells will likely be a useful indicator for forecasters. The fact that dual-polarimetric fields are similar in tropical and Midwest tornadic cases will also aid forecasters who irregularly experience landfalling tropical cyclone cases.

It should be noted, though, that this dataset alone is not robust enough to draw firm conclusions on dual-polarimetric differences between tornadic and non-tornadic cells. Further study of TC tornado cases should be undertaken including a comparison to cold season tornadoes in similar high shear and low CAPE environments in northern Alabama, as well as other dual-polarimetric studies. The suggestion of an ideal range for Z_{DR} (Kumjian and Ryzhkov 2008b) should also be studied for the larger dataset. Through further investigation of these storms, polarimetric signatures and distinctions between tornadic and non-tornadic cells can hopefully be identified to aid the operational community.

6. ACKNOWLEDGEMENTS

This work was supported by a Graduate Fellowship from the American Meteorological Society. Special thanks to the staff of the National Weather Service in Huntsville, Alabama, for help in completing this research.

7. RESOURCES

Baker, A.K., M.D. Parker, and M.D. Eastin, 2009: Environmental ingredients for supercells and tornadoes within Hurricane Ivan. *Wea. Forecasting*, **24**, 223-244.

Kumjian, M.R., and A. Ryzhkov, 2007: Polarimetric characteristics of tornadic and nontornadic supercell thunderstorms. Preprints, *33rd Conference on Radar Meteorology*, Cairns, Queensland, Ameri. Meteor. Soc., CD-ROM, P10.1.

---------, and ---------, 2008: Polarimetric signatures in supercell thunderstorms. *J. Appl. Meteor.*, **47**, 1940-1961.

---------, and ---------, 2008b: Microphysical differences between tornadic and nontornadic supercell rear-flank downdrafts revealed by dual-polarization radar measurements. Preprints, *24th Conference on Severe Local Storms*, Savannah, Georgia, Ameri. Meteor. Soc., CD-ROM, 3B.4.

---------, and ---------, 2009: Storm-relative helicity revealed from polarimetric radar measurements. *J. Atmos. Sci.*, **66**, 667-685.

Markowski, P.M., J.M. Straka, and E.N. Rasmussen, 2002: Direct surface thermodynamic observations within the rear-flank downdrafts of nontornadic and tornadic supercells. *Mon. Wea. Rev.*, **130**, 1692-1721.

McCaul, E.W. Jr. and M.L. Weisman, 1996: Simulations of shallow supercell storms in landfalling hurricane environments. *Mon. Wea. Rev.*, **124**, 408-429.

NCDC (National Climatic Data Center), cited 2009: NCDC Storm Events Database. [Available online at http://www4.ncdc.noaa.gov/cgi-win/wwcgi.dll?wwEvent~Storms]

Petersen, W.A., L.D. Carey, S.A. Rutledge, J.C. Knievel, N.J. Doesken, R.H. Johnson, T.B. McKee, T. Vonder Haar, and J.F. Weaver, 1999: Mesoscale and radar observations of the Fort Collins flash flood of 28 July 1997. *Bulletin of the AMS*, **80**, 191-216.

---------, K. Knupp, J. Walters, W. Deierling, M. Gauthier, B. Dolan, J.P. Dice, D. Satterfield, C. Davis, R. Blakeslee, S. Goodman, S. Podgorney, J. Hall, M. Budge, and A. Wooten, 2005: The UAH-NSSTC/WHNT ARMOR C-band dual-polarimetric radar: A unique collaboration in research, education and technology transfer. Preprints, *32nd Conference on Radar Meteorology*, Albuquerque, New Mexico, Ameri. Meteor. Soc., CD-ROM, 12R.4.

Romine, G.S., D.W. Burgess, and R.B. Wilhelmson, 2008: A dual-polarization-radar-based assessment of the 8 May 2003 Oklahoma City area tornadic supercell. *Mon. Wea. Rev.*, **136**, 2849-2870.